Supporting Information

HOW REACTIVE ARE DRUGGABLE CYSTEINES IN PROTEIN KINASES?

Ernest Awoonor-Williams and Christopher N. Rowley*

Department of Chemistry, Memorial University of Newfoundland, St. John's, NL, A1B 3X9, Canada

Table S1: Comparison of Calculated Cysteine pK_a's with Experimental pK_a values for Human Muscle Creatine Kinase (HMCK)

Protein Kinase	PDB ID	Cys Residue	Exptl. pK_a	RETI-pK_a[I]	PROPKA	H++
HMCK	1QK1	283	5.7 ± 0.1[1]	7.1 ± 0.6	9.9	6.8
HMCK (P284A)	1QK1	283	6.4 ± 0.1[1]	7.4 ± 0.8	9.7	6.9
HMCK (S285A)	1QK1	283	6.7 ± 0.1[2]	8.4 ± 0.4	10.6	7.5

[I] The calculated RETI-pKa's of Cys283 in HMCK is the average of independent 10 ns triplicate runs.

The pK_a's of the active site cysteine (Cys283) in wild-type and mutant variants of Human Muscle Creatine kinase (HMCK) is calculated using the replica-exchange thermodynamic integration (RETI) method—as a means of validation of the method within the kinase application domain. The implicit solvent models H++ and PROPKA are also used to compute the pK_a of the cysteine residue. The calculations are performed using coordinates from the model system of human ubiquitous mitochondrial protein kinase (PDB ID: 1QK1), as Naor and Jensen[3] have reported that the lower resolution structure (3.5 Å) of HMCK (PDB ID: 1I0E) gives erroneous results. The calculated cysteine pK_a's of Cys283 in the wild-type and mutant variants of HMCK are predicted in the correct pK_a direction by the RETI method, with an overall root-mean-square deviation (RMSD) of 1.4 pK units from experiment. The accuracy of the RETI method for this kinase domain is consistent with earlier validation studies where for a test set of 18 cysteine residues in 12 proteins, the overall RMSD was 2.4 pK units from experiment.[4] The H++ and PROPKA models are generally unreliable for predicting small relative pK differences in cysteine pK_a's (as seen in the range of predicted pK_a's for the wild-type and P284A HMCK mutant).

Table S2. Comparison of Computed pK_a's of Selected Kinase Cysteines using the different pK_a Calculation Methods

Protein Kinase	PDB ID	Cys Residue	RETI-pK_a[I]	CpH REMD-pK_a[II]	neMD/MC-pK_a[III]
c-KIT	3G0E	788	23.8 ± 1.0	20.2 ± 0.1	11.9 ± 0.7
c-Src	3F6X	277	8.4 ± 0.9	9.6 ± 0.0	9.3 ± 0.2
EGFR	4G5J	797	11.1 ± 0.7	13.5 ± 0.2	11.5 ± 0.3
JAK3	4QPS	909	13.0 ± 0.4	12.7 ± 0.4	11.1 ± 0.5
PDGFRα	5K5X	814	24.3 ± 0.6	19.4 ± 0.1	11.2 ± 0.1

[I, II, III] The calculated pK_a's are the average of three independent pK runs.

Table S2 lists the predicted pK_a's of targeted cysteines within select kinase models using the RETI and constant-pH methods (pH-REMD[5] and neMD/MC[6]). The predicted pK_a's generally agree well with one another, given that these methods are fundamentally different pK_a calculation methods. However, the predicted pK_a's of Cys788 in c-KIT and Cys814 in PDGFRα kinases using the hybrid neMD/MC method significantly differs from the pK_a's computed by the other methods. Both Cys788 and Cys814 residues are located in the catalytic loop segment of the kinases and are buried in the interior of the protein, as indicated by their low thiolate hydration numbers (Table S4). The neMD/MC sampling over the course of the 20-ns

* To whom correspondence should be addressed. Email: crowley@mun.ca

MD simulation draws in water molecules to stabilize the thiolate anion in these proteins, resulting in the rather different pK_a's observed. The predicted pK_a's still remain elevated for these proteins, and our primary conclusions are still valid. We note that these elevated predicted cysteine pK_a's are largely notional and not expected to be quantitative accurate. These elevated kinase cysteine pK_a's are suggestive of general trends and indicative of the physicochemical environment around the targetable cysteine residue. Figure S1 depicts the titration curves for both cysteines (i.e., Cys788 and Cys814) using the different constant-pH pK_a calculation methods.

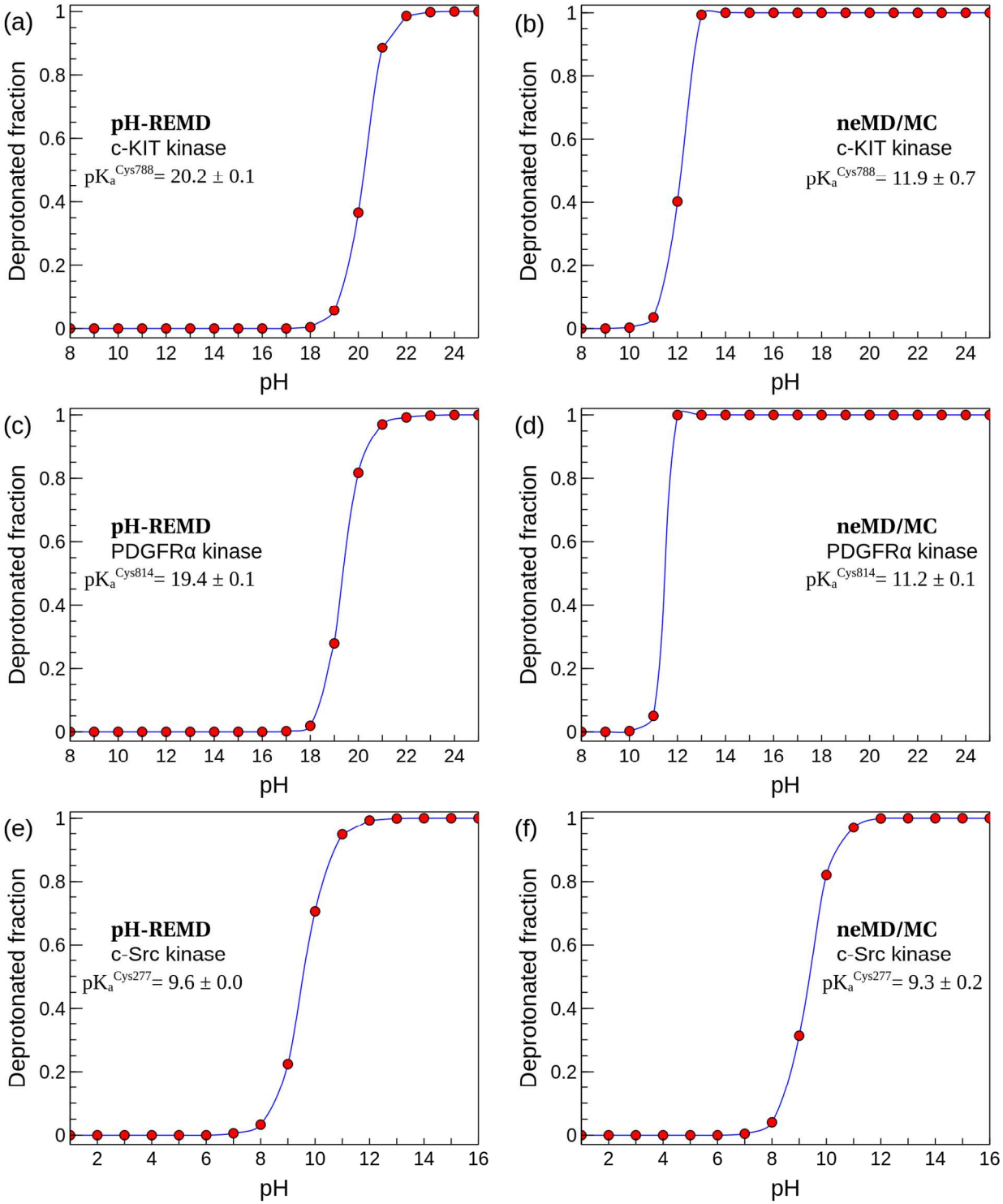

Figure S1. Titration curves of Cys788 (a, b), Cys814 (c, d), and Cys 277 (e, f) in c-KIT, PDGFRα, and c-Src kinases, respectively. The fitted curved were generated from deprotonated fractions of pH-REMD and hybrid neMD/MC constant pH molecular dynamics simulations. The reported pK_a's are the average of three independent replicates.

Table S3. Details of the Protein Kinase Structures Studied

Protein Kinase	PDB Code [a]	Cys Residue [b]	Region
BMX	3SXS [7]	496 [8]	Front pocket
BRAF	5FD2 [9]	532	Hinge region
BRAF (V600E)	5FD2 [9]	532	Hinge region
BTK	1K2P [10]	481 [11]	Front pocket
c-KIT "DFG-in"	1PKG [12]	788 [13]	Catalytic loop
c-KIT "DFG-out"	3G0E [14]	788 [13]	Catalytic loop
c-Src	3F6X [15]	277 [16]	P-loop
EGFR	4G5J [17]	797 [18]	Front pocket
EGFR (L858R)	4LQM [19]	797 [18]	Front pocket
EGFR (T790M)	4I24 [20]	797 [18]	Front pocket
EGFR (T790M/ L858R)	4I22 [20]	797 [18]	Front pocket
ERK2	4QTA [21]	166 [22]	DFG region
FGFR1	4UWY [23]	488 [24]	P-loop
FGFR4	4QQC [25]	477 [25]	P-loop
FGFR4	4XCU [26]	552 [26]	Hinge region
FLT3	4RT7 [27]	828 [28]	DFG region
GSK3B	3DU8 [29]	199 [30]	DFG region
HER2/ ErbB2	3PP0 [31]	805 [32]	Front pocket
HER3/ ErbB3	4OTW	721 [33]	Roof sheet
HER4/ ErbB4	3BCE [34]	778 [35]	Front pocket
IKK β	4KIK [36]	46 [37]	Catalytic loop
IKK β	4KIK [36]	179 [38]	Activation loop
ITK	4PQN [39]	442[40]	Front pocket
JAK3	4QPS [41]	909 [42]	Front pocket
JNK2	3E7O [43]	116 [44]	Front pocket
JNK3	4WHZ [45]	154 [44]	Front pocket
MEK1/ MAP2K1	1S9J [46]	207 [8]	DFG region
MSK1	3KN6 [47]	440	P-loop
NEK2	2W5A [48]	22 [49]	P-loop
PDGFR α	5K5X [50]	814 [13]	Catalytic loop
RSK1	3RNY [51]	432 [52]	P-loop
RSK2	2QR8 [53]	436 [52]	P-loop
TAK1	4GS6 [54]	174 [55]	DFG region
VEGFR2	4ASE [56]	1045 [57]	DFG region

[a] PDB Structure code, followed by the crystallographic structure reference (if one was published).
[b] Targeted cysteine residues and literature reference that provides confirmation of covalent modification of cysteines.

Table S4. Calculated pK_a's and Hydration numbers of Targeted Cysteine Residues using RETI-pK_a Method

Protein Kinase	Cys Residue	RETI-pK_a[I]	Hydration No.[II]
BMX	496	10.31 ± 0.46	3.91
BRAF	532	12.49 ± 0.65	4.42
BRAF (V600E)	532	11.36 ± 0.81	3.88
BTK	481	10.41 ± 0.80	4.26
c-KIT "DFG-in"	788	21.04 ± 0.48	4.62
c-KIT "DFG-out"	788	23.78 ± 1.03	3.59
c-Src	277	8.38 ± 0.88	5.98
EGFR	797	11.13 ± 0.65	4.26
EGFR (L858R)	797	12.58 ± 0.44	4.96
EGFR (T790M)	797	11.55 ± 0.97	4.25
EGFR (T790M/ L858R)	797	12.33 ± 0.59	4.70
ERK2	166	11.66 ± 0.67	4.01
FGFR1	488	11.02 ± 0.86	4.98
FGFR4	477	7.79 ± 0.73	4.40
FGFR4	552	9.07 ± 0.78	4.06
FLT3	828	15.11 ± 0.54	4.29
GSK3B	199	12.41 ± 0.83	4.24
HER2/ ErbB2	805	11.82 ± 0.47	3.78
HER3/ ErbB3	721	12.25 ± 0.73	4.96
HER4/ ErbB4	778	12.36 ± 0.85	3.96
IKKβ	46	11.37 ± 0.83	4.29
IKKβ	179	10.76 ± 0.94	3.90
ITK	442	11.96 ± 0.55	3.57
JAK3	909	13.00 ± 0.39	5.39
JNK2	116	7.01 ± 0.83	5.53
JNK3	154	9.62 ± 0.51	5.11
MEK1/ MAP2K1	207	12.77 ± 0.42	3.95
MSK1	440	14.80 ± 0.41	5.29
NEK2	22	12.59 ± 0.62	4.84
PDGFRα	814	24.34 ± 0.58	3.68
RSK1	432	12.25 ± 0.49	4.79
RSK2	436	12.61 ± 0.68	5.25
TAK1	174	13.60 ± 0.55	4.98
VEGFR2	1045	15.28 ± 0.43	4.15

[I, II] The pK_a's of the druggable cysteines and hydration numbers of the thiolates are the average of independent 10 ns runs performed in triplicate. Cysteine thiolate hydration numbers were computed from the trajectories of each independent free energy calculation. For the model cysteine in aqueous solution, the hydration number calculated was 4.44.

Table S5. List of Charged Residues within 10 Å from Target Cysteine Residue

Protein Kinase	Cys Residue	Acidic Residues [Å]	Basic Residues [Å]
BMX	496	---	Arg502 [8.76], Arg540[9.20]
BRAF	532	Glu533[8.52], Glu586[9.55]	His585[5.60], Lys591[6.44]
BRAF (V600E)	532	Glu533[8.52], Glu586[9.55]	His585[5.60], Lys591[6.44]
BTK	481	Glu488[9.05], Asp539[9.80]	Arg487[8.08], Arg525[9.23]
c-KIT "DFG-in"	788	Asp816[4.26], Asp572[7.35], Asp851[9.74]	Lys786[8.10]
c-KIT "DFG-out"	788	Asp851[7.96]	His790[8.75], Arg791[9.74]
c-Src	277	---	----
EGFR	797	Asp800[3.42]	Arg803[8.34], Arg841[9.80]
EGFR (L858R)	797	Asp800[3.52], Glu804[8.64]	Arg803[7.73], Arg841[9.39]
EGFR (T790M)	797	Asp800[3.53], Glu804[8.60]	Asp803[7.84], Arg841[9.66]
EGFR (T790M/ L858R)	797	Asp800[3.64], Glu804[8.81]	Arg803[7.56], Arg841[9.48]
ERK2	166	Asp167[6.10], Glu71[7.55], Asp111[7.64], Asp149[9.51]	Lys54[6.58], His147[7.36], Lys151[9.02]
FGFR1	488	Asp524[6.04], Asp519[7.52], Asp527[9.17]	Lys517[5.31], Lys655[7.83], Lys523[8.00]
FGFR4	477	Glu475[5.04], Asp641[8.72]	Lys644[6.11], Lys506[8.69], Lys503[8.95]
FGFR4	552	Glu485[8.91], Glu551[9.86]	Arg483[6.50]
FLT3	828	Asp829[6.61], Asp698[8.06], Asp811[9.34], Glu661[9.78]	Arg834[7.09], His809[7.21], Lys644[7.81]
GSK3B	199	Asp200[5.61], Glu97[9.29], Asp181[9.37]	His179[7.23], Lys85[7.53], Lys183[8.69]
HER2/ ErbB2	805	Asp808[4.08]	Arg811[7.94], Arg849[9.35]
HER3/ ErbB3	721	---	Lys706[8.70], Lys723[9.03], His705[9.14]
HER4/ ErbB4	778	Glu781[3.71], Glu785[8.80]	Arg822[9.59]
IKKβ	46	Asp90[8.02], Glu61[9.67]	Arg55[8.40], Arg47[9.77], Lys44[9.80]
IKKβ	179	---	Arg144[5.15], Lys171[6.29]
ITK	442	Asp445[3.42]	Arg448[7.39]
JAK3	909	Asp912[3.26]	Arg911[4.67], Arg953[5.59], Arg916[8.71]
JNK2	116	Glu217[7.77]	His120[8.18], Lys153[9.85]
JNK3	154	Glu255[7.26]	Lys191[10.27], His259[12.19]
MEK1/ MAP2K1	207	Asp208[3.99], Asp190[8.66]	Lys97[5.95], His188[6.72], Lys192[9.63]
MSK1	440	Asp565[8.33]	Lys455[8.00], Arg441[9.73]
NEK2	22	Asp159[8.24], Glu38[9.56]	Lys37[5.14]
PDGFRα	814	Asp877[7.96]	His816[8.38], Arg817[9.70], His650[9.89]
RSK1	432	Glu431[6.53], Asp557[7.85]	Lys447[6.11]
RSK2	436	Asp427[8.84]	Lys451[7.77]
TAK1	174	Asp175[5.25], Glu77[8.63], Asp156[9.39]	His154[7.21], Lys63[7.63]
VEGFR2	1045	Glu967[8.06], Asp1046[8.42], Glu935[9.97]	His1026[8.35], Lys1043[8.43], Lys918[9.02], Arg1051[9.66]

Table S6. Comparison of the pK_a's of Cysteine Residues in Protein Kinases

Protein Kinase	Cys Residue	RETI-pK_a[I]	PROPKA	H++
BMX	496	10.31 ± 0.46	9.92	10.42
BRAF	532	12.49 ± 0.65	11.24	>12
BRAF (V600E)	532	11.36 ± 0.81	11.24	>12
BTK	481	10.41 ± 0.80	9.44	9.74
c-KIT "DFG-in"	788	21.04 ± 0.48	12.67	>12
c-KIT "DFG-out"	788	23.78 ± 1.03	13.00	>12
c-Src	277	8.38 ± 0.88	9.14	8.10
EGFR	797	11.13 ± 0.65	10.38	10.55
EGFR (L858R)	797	12.58 ± 0.44	11.17	11.58
EGFR (T790M)	797	11.55 ± 0.97	11.02	10.70
EGFR (T790M/ L858R)	797	12.33 ± 0.59	11.43	11.74
ERK2	166	11.66 ± 0.67	12.73	>12
FGFR1	488	11.02 ± 0.86	9.32	8.77
FGFR4	477	7.79 ± 0.73	10.00	10.99
FGFR4	552	9.07 ± 0.78	10.12	9.45
FLT3	828	15.11 ± 0.54	13.11	>12
GSK3B	199	12.41 ± 0.83	12.39	11.79
HER2/ ErbB2	805	11.82 ± 0.47	10.65	10.72
HER3/ ErbB3	721	12.25 ± 0.73	10.85	10.44
HER4/ ErbB4	778	12.36 ± 0.85	10.62	10.38
IKKβ	46	11.37 ± 0.83	9.75	>12
IKKβ	179	10.76 ± 0.94	10.85	>12
ITK	442	11.96 ± 0.55	9.68	10.42
JAK3	909	13.00 ± 0.39	10.37	9.10
JNK2	116	7.01 ± 0.83	10.24	9.53
JNK3	154	9.62 ± 0.51	10.56	9.77
MEK1/ MAP2K1	207	12.77 ± 0.42	13.48	>12
MSK1	440	14.80 ± 0.41	11.05	10.66
NEK2	22	12.59 ± 0.62	10.74	9.34
PDGFRα	814	24.34 ± 0.58	12.92	>12
RSK1	432	12.25 ± 0.49	10.88	>12
RSK2	436	12.61 ± 0.68	10.91	10.36
TAK1	174	13.60 ± 0.55	12.88	>12
VEGFR2	1045	15.28 ± 0.43	13.56	>12

[I] The pK_a's of the druggable cysteines reported are the average of independent 10 ns runs performed in triplicate.

Table S7. Calibration of constant pH-REMD method with the Model Cysteine Pentapeptide

Method	pK_a
Experimental [58]	8.55 ± 0.03
pH-REMD (Amber ff99SB)	8.74 ± 0.02

The pH-REMD method with the Amber99 force field has been reported to yield accurate titratable residue pK_a's for both model peptides and benchmark protein systems.[5] We validated the use of the Amberff99SB force field with the pH-REMD approach by computing the pK_a of the model cysteine pentapeptide (i.e., ACE–$(Ala)_2$–Cys–$(Ala)_2$–NH_2). Three independent pH-REMD simulation trials were performed on the model system. Each pH-REMD trial simulation consisted of 8 replicas spanning pH range of 6.5–10.0, with increments of 0.5 pH units. Simulation cell was modeled to mimic experimental conditions[58] and pH-REMD parameters chosen were the same as those adopted for kinase model systems (see Constant pH-REMD in Theory and Methods). Each replica window was run for 20 ns, equaling a total of 160 ns for each independent model system run. The average predicted pK_a from the triplicate run of the cysteine pentapeptide is reported in Table S7. This computed pK_a is in close agreement with the experimental reported pK_a. For this reason, we believe the Amberff99SB force field is an appropriate choice for use in the constant pH-REMD simulations of selected kinase model systems, having been originally implemented and parameterized using the AMBER program.

Sample Input Parameters for RETI Molecular Dynamics Simulations

1) Energy Minimization Parameters

```
; Parameters describing what to do, when to stop and what to save
integrator      = steep         ; Algorithm (steep = steepest descent minimization)
emtol           = 1000.0        ; Stop minimization when the maximum force < 1000.0 kJ/mol/nm
emstep      = 0.01              ; Energy step size
nsteps          = 100000        ; Maximum number of (minimization) steps to perform
; Parameters describing how to find the neighbors of each atom and how to calculate the interactions
nstlist         = 1             ; Frequency to update the neighbor list and long range forces
cutoff-scheme   = Verlet
ns_type             = grid      ; Method to determine neighbor list (simple, grid)
coulombtype     = PME           ; Treatment of long range electrostatic interactions
rcoulomb        = 1.0           ; Short-range electrostatic cut-off
rvdw            = 1.0           ; Short-range Van der Waals cut-off
pbc             = xyz           ; Periodic Boundary Conditions (yes/no)
```

2) NVT Equilibration Parameters

```
title           =  NVT equilibration
define          = -DPOSRES      ; position restrain the protein
; Run parameters
integrator      = sd            ; leap-frog integrator
nsteps          = 10000000    ; 2 * 500000 = 10000 ps
dt              = 0.002         ; 2 fs
; Output control
nstxout             = 10000     ; save coordinates every 1.0 ps
nstvout             = 10000     ; save velocities every 1.0 ps
```

```
nstenergy        = 10000              ; save energies every 1.0 ps
nstlog           = 10000              ; update log file every 1.0 ps
; Bond parameters
continuation           = no                    ; first dynamics run
constraint_algorithm   = lincs          ; holonomic constraints
constraints            = all-bonds; all bonds (even heavy atom-H bonds) constrained
lincs_iter             = 1                     ; accuracy of LINCS
lincs_order            = 4                     ; also related to accuracy
; Neighborsearching
cutoff-scheme   = Verlet
ns_type                = grid           ; search neighboring grid cells
nstlist          = 10              ; 20 fs, largely irrelevant with Verlet
rcoulomb         = 1.0             ; short-range electrostatic cutoff (in nm)
rvdw             = 1.0             ; short-range van der Waals cutoff (in nm)
; Electrostatics
coulombtype      = PME             ; Particle Mesh Ewald for long-range electrostatics
pme_order        = 4               ; cubic interpolation
fourierspacing   = 0.16    ; grid spacing for FFT
; Temperature coupling is on
tcoupl           = V-rescale               ; modified Berendsen thermostat
tc-grps          = Protein Non-Protein     ; two coupling groups - more accurate
tau_t            = 0.1       0.1          ; time constant, in ps
ref_t            = 298.15          298.15          ; reference temperature, one for each group, in K
; Pressure coupling is off
pcoupl           = no              ; no pressure coupling in NVT
; Periodic boundary conditions
pbc              = xyz                ; 3-D PBC
; Dispersion correction
DispCorr         = EnerPres          ; account for cut-off vdW scheme
; Velocity generation
gen_vel                = yes             ; assign velocities from Maxwell distribution
gen_temp         = 300             ; temperature for Maxwell distribution
gen_seed         = -1              ; generate a random seed
```

3) NPT Equilibration Parameters

```
title            =  NPT equilibration
define           = -DPOSRES       ; position restrain the protein
; Run parameters
integrator       = sd              ; leap-frog integrator
nsteps           = 10000000                ; 2 * 10000000 = 10000 ps
dt                 = 0.002                 ; 2 fs
; Output control
nstxout                = 10000           ; save coordinates every 20.0 ps
nstvout                = 10000           ; save velocities every 20.0 ps
nstenergy        = 10000           ; save energies every 20.0 ps
nstlog           = 10000           ; update log file every 20.0 ps
; Bond parameters
continuation           = yes                   ; Restarting after NVT
constraint_algorithm   = lincs          ; holonomic constraints
```

```
constraints              = all-bonds; all bonds (even heavy atom-H bonds) constrained
lincs_iter               = 1                    ; accuracy of LINCS
lincs_order              = 4                    ; also related to accuracy
; Neighborsearching
cutoff-scheme   = Verlet
ns_type                  = grid          ; search neighboring grid cells
nstlist          = 10    ; 20 fs, largely irrelevant with Verlet scheme
rcoulomb         = 1.0           ; short-range electrostatic cutoff (in nm)
rvdw             = 1.0           ; short-range van der Waals cutoff (in nm)
; Electrostatics
coulombtype      = PME                  ; Particle Mesh Ewald for long-range electrostatics
pme_order        = 4               ; cubic interpolation
fourierspacing   = 0.16          ; grid spacing for FFT
; Temperature coupling is on
tcoupl           = V-rescale             ; modified Berendsen thermostat
tc-grps          = Protein Non-Protein       ; two coupling groups - more accurate
tau_t            = 0.1    0.1           ; time constant, in ps
ref_t            = 298.15  298.15   ; reference temperature, one for each group, in K
; Pressure coupling is on
pcoupl           = Parrinello-Rahman     ; Pressure coupling on in NPT
pcoupltype       = isotropic          ; uniform scaling of box vectors
tau_p            = 1.0                        ; time constant, in ps
ref_p            = 1.0                        ; reference pressure, in bar
compressibility  = 4.5e-5                ; isothermal compressibility of water, bar^-1
refcoord_scaling  = com
; Periodic boundary conditions
pbc              = xyz           ; 3-D PBC
; Dispersion correction
DispCorr         = EnerPres          ; account for cut-off vdW scheme
; Velocity generation
gen_vel                  = no            ; Velocity generation is off
```

4) Free Energy Calculation Parameters

```
integrator          = sd
dt                = 0.002
nsteps            = 6000000
nstxout           = 5000
nstvout           = 5000
nstlog            = 5000
nstenergy         = 250
;nstxout-compressed      = 250
rlist             = 1.0
coulombtype         = PME
pme_order         = 6
fourierspacing = 0.1
cutoff-scheme   = Verlet
ns_type = grid       ; search neighboring grid cells
nstlist    = 10      ; 20 fs, largely irrelevant with Verlet
rcoulomb          = 1.0
```

```
rvdw                    = 1.0
; and pressure to 1 bar
pcoupl = parrinello-rahman
ref-p = 1
compressibility = 4.5e-5
tau-p = 5
gen-vel                 = $GEN_VEL$
gen-temp                = 300
gen-seed                = 173529
constraints             = hbonds
constraint_algorithm =  lincs
lincs-order =  12
tc_grps            =  System
tau_t              =  1.0
ld_seed            =  -1
ref_t = 298.15

; Free energy
free_energy = yes
init-lambda-state = $STATE$
calc-lambda-neighbors = -1
sc_alpha = 0.0
couple-lambda1 = vdw-q
fep-lambdas = $ALL_LAMBDAS$
coul-lambdas = $ALL_LAMBDAS$
vdw-lambdas = $ALL_LAMBDAS$
DispCorr = EnerPres
```

Sample Input Files for the constant pH-REMD Simulations

1) Energy Minimization Parameters

```
Minimize for constant pH REMD simulations
&cntrl
  imin=1,
  ncyc=1000,
  maxcyc=5000,
  ntpr=50,
  cut=8,
  restraintmask='!:WAT&@CA,C,O,N'
  restraint_wt=10.0,
 /
```

2) Heating Parameters

```
Heating step for constant pH REMD simulations
&cntrl
  imin=0, irest=0, ntx=1,
  ntpr=1000, ntwx=1000, nstlim=200000,
  dt=0.002, ntt=3, gamma_ln=5.0, ig=-1,
  ntc=2, ntf=2, cut=8, ntb=1,
```

```
  iwrap=1, ioutfm=1, nmropt=1,
 /
 &wt
  TYPE='TEMP0', ISTEP1=0, ISTEP2=150000,
  VALUE1=10.0, VALUE2=300.0,
 /
 &wt TYPE='END' /
```

3) Equilibration/Relaxation Parameters

```
Explicit solvent molecular dynamics constant pressure MD
 &cntrl
  imin=0, irest=1, ntx=5,
  ntpr=1000, ntwx=1000, nstlim=5000000,
  dt=0.002, ntt=3, tempi=300,
  temp0=300, gamma_ln=1.0, ig=-1,
  ntp=1, ntc=2, ntf=2, cut=8,
  ntb=2, iwrap=1, ioutfm=1,
 /
```

4) Constant pH-REMD Parameters for one replica (pH=12)

```
Explicit REMD for cpH
 &cntrl
  imin=0, irest=1, ntx=5, ntxo=2,
  ntpr=1000, ntwx=1000, nstlim=5000,
  dt=0.002, ntt=3, numexchg=1000, tempi=300.0,
  temp0=300.0, gamma_ln=5.0, ig=-1,
  ntc=2, ntf=2, cut=8, iwrap=1,
  ioutfm=1, icnstph=2, ntcnstph=100,
  solvph=12.0, ntrelax=100, saltcon=0.1,
 /
```

Sample Input Files for the constant-pH neMD/MC Simulations

1) Equilibration Parameters

```
# input
coordinates          egfr-ionized.pdb
structure            egfr-ionized.psf
parameters           par_all36_prot_mod.prm
paratypecharmm       on

# output
set output           egfr_equil
outputname           $output
dcdfile              ${output}.dcd
xstFile              ${output}.xst
dcdfreq              10000
xstFreq              1000
binaryoutput         yes
binaryrestart        yes
```

```
outputEnergies          100
restartfreq            1000
fixedAtoms              off
rigidBonds              all

# Basic dynamics
exclude                scaled1-4
1-4scaling              1
COMmotion               no
dielectric             1.0

# Simulation space partitioning
switching               on
switchdist              10
cutoff                 12
pairlistdist            14

# Multiple timestepping
firsttimestep           0
timestep                2
stepspercycle           20
nonbondedFreq           1
fullElectFrequency      2

# Temperature control
set temperature         298.15
temperature             $temperature;  # initial temperature

# Langevin Dynamics
langevin                on;            # do langevin dynamics
langevinDamping         1;             # damping coefficient (gamma) of 1/ps
langevinTemp            $temperature;   # bath temperature
langevinHydrogen        no;             # don't couple langevin bath to hydrogens
seed                   12345

# Pressure control
langevinPiston          on
langevinPistonTarget    1.01325; # in bar -> 1.01325 bar = 1 atm
langevinPistonPeriod    2000
langevinPistonDecay     100
langevinPistonTemp      $temperature
useFlexibleCell         no
UseGroupPressure        yes
fixedAtomsForces        off

# PBC
cellBasisVector1        82.2 0.0 0.0
cellBasisVector2        0.0 87.6 0.0
cellBasisVector3        0.0 0.0 79.5
cellOrigin              65.7 5.7 -22.4
```

```
wrapAll                on
dcdUnitCell            yes
PME                    yes
PMEGridSpacing         1.0

# Scripting
minimize            1000
reinitvels          $temperature
run                 10000000
```

2) Constant-pH Specific Parameters

```
# These keywords all follow as usual
set temperature 298.15
set topo_dir "../topology"
structure $topo_dir/egfr-ionized.psf
coordinates $topo_dir/egfr-ionized.pdb
binCoordinates $topo_dir/egfr_equil.coor
binVelocities  $topo_dir/egfr_equil.vel
extendedSystem $topo_dir/egfr_equil.xsc

wrapWater on
wrapAll on
wrapNearest on
outputEnergies 5000
DCDFreq 5000

timestep 2.0
fullElectFrequency 2
rigidBonds ALL
langevin on
langevinTemp $temperature
langevinDamping 1.0
langevinHydrogen no

switching on
VDWForceSwitching on
LJCorrection on
switchDist 10.0
cutoff 12.0
pairlistDist 14.0
exclude scaled1-4
1-4scaling 1.0
PME on
PMEGridSpacing 1.0

# Begin constant-pH MD keywords and modifications
# Load the constant-pH Tcl files
source ../namdcph/namdcph.tcl
# Load force field files as usual, but add constant-pH specific parameters
```

```
set toppar_dir "../toppar"
paratypecharmm on
parameters $toppar_dir/par_all36_prot.prm
#parameters par_all36m_prot.prm
parameters $toppar_dir/par_cph36_prot.prm
parameters $toppar_dir/par_all36_solvent.prm
# Load constant-pH specific topology files
cphConfigFile $toppar_dir/conf_cph36_prot.json
topology $toppar_dir/top_all36_prot.rtf
topology $toppar_dir/top_cph36_prot.rtf
topology $toppar_dir/top_solvent.rtf

# We will be running multiple pH values sorted into their own directories, but
# otherwise using the same naming scheme.
source pH.tcl
#set pHList [list 6.0 6.5 7.0 7.5 8.0 8.5 9.0 9.5 10.0 10.5 11.0 11.5]
#set pH [lindex $pHList [myReplica]]
pH $pH

outputname prot_prod0
stdout prot_prod0.log
cphMDBasename namdcph.md
cphSwitchBasename namdcph.sw

# Experimental values from
# For clarity, each residue is sorted by type with a separate command:
# CYS
cphSetResiduepKai AP1:797 9.5
cphSetResiduepKai AP1:800 4.0
cphProposalWeight AP1:797 10.0
cphProposalWeight AP1:800 10.0

# With the current settings this implies 10 ps between switching attempts,
# which will be 15 ps in length. These settings should be relatively close to
# optimal.
cphNumstepsPerSwitch 7500
cphRun 5000 2000
# Don't exit until all simulations have finished.
#replicaBarrier
exit
```

REFERENCES

(1) Wang, P.-F.; Flynn, A. J.; Naor, M. M.; Jensen, J. H.; Cui, G.; Merz, K. M.; Kenyon, G. L.; McLeish, M. J. Exploring the Role of the Active Site Cysteine in Human Muscle Creatine Kinase †. *Biochemistry* **2006**, *45* (38), 11464–11472.

(2) Wang, P.-F.; McLeish, M. J.; Kneen, M. M.; Lee, G.; Kenyon, G. L. An Unusually Low p K a for Cys282 in the Active Site of Human Muscle Creatine Kinase †. *Biochemistry* **2001**, *40* (39), 11698–11705.

(3) Naor, M. M.; Jensen, J. H. Determinants of Cysteine PKa Values in Creatine Kinase and Alpha1-Antitrypsin. *Proteins* **2004**, *57* (4), 799–803.
(4) Awoonor-Williams, E.; Rowley, C. N. Evaluation of Methods for the Calculation of the PKa of Cysteine Residues in Proteins. *J. Chem. Theory Comput.* **2016**, *12* (9), 4662–4673.
(5) Swails, J. M.; York, D. M.; Roitberg, A. E. Constant PH Replica Exchange Molecular Dynamics in Explicit Solvent Using Discrete Protonation States: Implementation, Testing, and Validation. *J. Chem. Theory Comput.* **2014**, *10* (3), 1341–1352.
(6) Radak, B. K.; Chipot, C.; Suh, D.; Jo, S.; Jiang, W.; Phillips, J. C.; Schulten, K.; Roux, B. Constant-PH Molecular Dynamics Simulations for Large Biomolecular Systems. *J. Chem. Theory Comput.* **2017**, *13* (12), 5933–5944.
(7) Muckelbauer, J.; Sack, J. S.; Ahmed, N.; Burke, J.; Chang, C. Y.; Gao, M.; Tino, J.; Xie, D.; Tebben, A. J. X-Ray Crystal Structure of Bone Marrow Kinase in the X Chromosome: A Tec Family Kinase. *Chem. Biol. Drug Des.* **2011**, *78* (5), 739–748.
(8) Liu, Q.; Sabnis, Y.; Zhao, Z.; Zhang, T.; Buhrlage, S. J.; Jones, L. H.; Gray, N. S. Developing Irreversible Inhibitors of the Protein Kinase Cysteinome. *Chem. Biol.* **2013**, *20* (2), 146–159.
(9) Liu, L.; Lee, M. R.; Kim, J. L.; Whittington, D. A.; Bregman, H.; Hua, Z.; Lewis, R. T.; Martin, M. W.; Nishimura, N.; Potashman, M.; et al. Purinylpyridinylamino-Based DFG-in/AC-Helix-out B-Raf Inhibitors: Applying Mutant versus Wild-Type B-Raf Selectivity Indices for Compound Profiling. *Bioorg. Med. Chem.* **2016**, *24* (10), 2215–2234.
(10) Mao, C.; Zhou, M.; Uckun, F. M. Crystal Structure of Bruton's Tyrosine Kinase Domain Suggests a Novel Pathway for Activation and Provides Insights into the Molecular Basis of X-Linked Agammaglobulinemia. *J. Biol. Chem.* **2001**, *276* (44), 41435–41443.
(11) Marcotte, D. J.; Liu, Y. T.; Arduini, R. M.; Hession, C. A.; Miatkowski, K.; Wildes, C. P.; Cullen, P. F.; Hong, V.; Hopkins, B. T.; Mertsching, E.; et al. Structures of Human Bruton's Tyrosine Kinase in Active and Inactive Conformations Suggest a Mechanism of Activation for TEC Family Kinases. *Protein Sci.* **2010**, *19* (3), 429–439.
(12) Mol, C. D.; Lim, K. B.; Sridhar, V.; Zou, H.; Chien, E. Y. T.; Sang, B. C.; Nowakowski, J.; Kassel, D. B.; Cronin, C. N.; McRee, D. E. Structure of a C-Kit Product Complex Reveals the Basis for Kinase Transactivation. *J. Biol. Chem.* **2003**, *278* (34), 31461–31464.
(13) Leproult, E.; Barluenga, S.; Moras, D.; Wurtz, J.-M.; Winssinger, N. Cysteine Mapping in Conformationally Distinct Kinase Nucleotide Binding Sites: Application to the Design of Selective Covalent Inhibitors. *J. Med. Chem.* **2011**, *54* (5), 1347–1355.
(14) Gajiwala, K. S.; Wu, J. C.; Christensen, J.; Deshmukh, G. D.; Diehl, W.; DiNitto, J. P.; English, J. M.; Greig, M. J.; He, Y.-A.; Jacques, S. L.; et al. KIT Kinase Mutants Show Unique Mechanisms of Drug Resistance to Imatinib and Sunitinib in Gastrointestinal Stromal Tumor Patients. *Proc. Natl. Acad. Sci.* **2009**, *106* (5), 1542–1547.
(15) Statsuk, A. V.; Maly, D. J.; Seeliger, M. A.; Fabian, M. A.; Biggs, W. H.; Lockhart, D. J.; Zarrinkar, P. P.; Kuriyan, J.; Shokat, K. M. Tuning a Three-Component Reaction For Trapping Kinase Substrate Complexes. *J. Am. Chem. Soc.* **2008**, *130* (51), 17568–17574.
(16) Kwarcinski, F. E.; Fox, C. C.; Steffey, M. E.; Soellner, M. B. Irreversible Inhibitors of C-Src Kinase That Target a Nonconserved Cysteine. *ACS Chem. Biol.* **2012**, *7* (11), 1910–1917.
(17) Solca, F.; Dahl, G.; Zoephel, A.; Bader, G.; Sanderson, M.; Klein, C.; Kraemer, O.; Himmelsbach, F.; Haaksma, E.; Adolf, G. R. Target Binding Properties and Cellular Activity of Afatinib (BIBW 2992), an Irreversible ErbB Family Blocker. *J. Pharmacol. Exp. Ther.* **2012**, *343* (2), 342–350.
(18) Fry, D. W.; Bridges, A. J.; Denny, W. A.; Doherty, A.; Greis, K. D.; Hicks, J. L.; Hook, K. E.; Keller, P. R.; Leopold, W. R.; Loo, J. A.; et al. Specific, Irreversible Inactivation of the Epidermal Growth Factor Receptor and ErbB2, by a New Class of Tyrosine Kinase Inhibitor. *Proc. Natl. Acad. Sci.* **1998**, *95* (20), 12022–12027.
(19) Yasuda, H.; Park, E.; Yun, C.-H.; Sng, N. J.; Lucena-Araujo, A. R.; Yeo, W.-L.; Huberman, M. S.; Cohen, D. W.; Nakayama, S.; Ishioka, K.; et al. Structural, Biochemical, and Clinical Characterization of Epidermal Growth Factor Receptor (EGFR) Exon 20 Insertion Mutations in Lung Cancer. *Sci. Transl. Med.* **2013**, *5* (216), 216ra177-216ra177.
(20) Gajiwala, K. S.; Feng, J.; Ferre, R.; Ryan, K.; Brodsky, O.; Weinrich, S.; Kath, J. C.; Stewart, A. Insights into the Aberrant Activity of Mutant EGFR Kinase Domain and Drug Recognition. *Structure* **2013**, *21* (2), 209–219.
(21) Chaikuad, A.; M C Tacconi, E.; Zimmer, J.; Liang, Y.; Gray, N. S.; Tarsounas, M.; Knapp, S. A Unique Inhibitor Binding Site in ERK1/2 Is Associated with Slow Binding Kinetics. *Nat. Chem. Biol.* **2014**, *10* (10), 853–860.
(22) Ward, R. A.; Colclough, N.; Challinor, M.; Debreczeni, J. E.; Eckersley, K.; Fairley, G.; Feron, L.; Flemington, V.; Graham, M. A.; Greenwood, R.; et al. Structure-Guided Design of Highly Selective and Potent Covalent Inhibitors of ERK1/2. *J. Med. Chem.* **2015**, *58* (11), 4790–4801.
(23) Bunney, T. D.; Wan, S.; Thiyagarajan, N.; Sutto, L.; Williams, S. V.; Ashford, P.; Koss, H.; Knowles, M. A.; Gervasio, F. L.; Coveney, P. V.; et al. The Effect of Mutations on Drug Sensitivity and Kinase Activity of Fibroblast Growth Factor Receptors: A Combined Experimental and Theoretical Study. *EBioMedicine* **2015**, *2* (3), 194–204.
(24) Zhou, W.; Hur, W.; McDermott, U.; Dutt, A.; Xian, W.; Ficarro, S. B.; Zhang, J.; Sharma, S. V.; Brugge, J.; Meyerson, M.; et al. A Structure-Guided Approach to Creating Covalent FGFR Inhibitors. *Chem. Biol.* **2010**, *17* (3), 285–295.
(25) Tan, L.; Wang, J.; Tanizaki, J.; Huang, Z.; Aref, A. R.; Rusan, M.; Zhu, S.-J.; Zhang, Y.; Ercan, D.; Liao, R. G.; et al. Development of Covalent Inhibitors That Can Overcome Resistance to First-Generation FGFR Kinase Inhibitors. *Proc. Natl. Acad. Sci.* **2014**, *111* (45), E4869–E4877.
(26) Hagel, M.; Miduturu, C.; Sheets, M.; Rubin, N.; Weng, W.; Stransky, N.; Bifulco, N.; Kim, J. L.; Hodous, B.; Brooijmans, N.; et al. First Selective Small Molecule Inhibitor of FGFR4 for the Treatment of Hepatocellular Carcinomas with an Activated FGFR4 Signaling Pathway. *Cancer Discov.* **2015**, *5* (4), 424–437.
(27) Smith, C. C.; Zhang, C.; Lin, K. C.; Lasater, E. A.; Zhang, Y.; Massi, E.; Damon, L. E.; Pendleton, M.; Bashir, A.; Sebra, R.; et al. Characterizing and Overriding the Structural Mechanism of the Quizartinib-Resistant FLT3 "Gatekeeper" F691L Mutation with PLX3397. *Cancer Discov.* **2015**, *5* (6), 668–679.
(28) Versele, M.; Haefner, B.; Wroblowski, B.; Stansfield, I.; Mevellec, L.; Gilissen, R.; Neumann, L.; Augustin, M.; Jacobs, K.; Cools, J.; et al. Abstract 4800: Covalent Flt3-Cys828 Inhibition Represents a Novel Therapeutic Approach for the Treatment of Flt3-ITD and Flt3-D835 Mutant Acute Myeloid Leukemia. *Cancer Res.* **2016**, *76* (14 Supplement), 4800–4800.
(29) Menichincheri, M.; Bargiotti, A.; Berthelsen, J.; Bertrand, J. A.; Bossi, R.; Ciavolella, A.; Cirla, A.; Cristiani, C.; Croci, V.; D'Alessio, R.; et al. First Cdc7 Kinase Inhibitors: Pyrrolopyridinones as Potent and Orally Active Antitumor Agents. 2. Lead Discovery †. *J. Med. Chem.* **2009**, *52* (2), 293–307.
(30) Domínguez, J. M.; Fuertes, A.; Orozco, L.; del Monte-Millán, M.; Delgado, E.; Medina, M. Evidence for Irreversible Inhibition of Glycogen Synthase Kinase-3β by Tideglusib. *J. Biol. Chem.* **2012**, *287* (2), 893–904.
(31) Aertgeerts, K.; Skene, R.; Yano, J.; Sang, B. C.; Zou, H.; Snell, G.; Jennings, A.; Iwamoto, K.; Habuka, N.; Hirokawa, A.; et al. Structural Analysis of the Mechanism of Inhibition and Allosteric Activation of the Kinase Domain of HER2 Protein. *J. Biol. Chem.* **2011**, *286* (21), 18756–18765.
(32) Rabindran, S. K.; Discafani, C. M.; Rosfjord, E. C.; Baxter, M.; Floyd, M. B.; Golas, J.; Hallett, W. A.; Johnson, B. D.; Nilakantan, R.; Overbeek, E.; et al. Antitumor Activity of HKI-272, an Orally Active, Irreversible Inhibitor of the HER-2 Tyrosine Kinase. *Cancer Res.* **2004**, *64* (11), 3958–3965.
(33) Xie, T.; Lim, S. M.; Westover, K. D.; Dodge, M. E.; Ercan, D.; Ficarro, S. B.; Udayakumar, D.; Gurbani, D.; Tae, H. S.; Riddle, S. M.; et al. Pharmacological Targeting of the Pseudokinase Her3. *Nat. Chem. Biol.* **2014**, *10* (12), 1006–1012.
(34) Qiu, C.; Tarrant, M. K.; Choi, S. H.; Sathyamurthy, A.; Bose, R.; Banjade, S.; Pal, A.; Bornmann, W. G.; Lemmon, M. A.; Cole, P. A.; et al. Mechanism of Activation and Inhibition of the HER4/ErbB4 Kinase. *Structure* **2008**, *16* (3), 460–467.

(35) Modjtahedi, H.; Cho, B. C.; Michel, M. C.; Solca, F. A Comprehensive Review of the Preclinical Efficacy Profile of the ErbB Family Blocker Afatinib in Cancer. *Naunyn. Schmiedebergs. Arch. Pharmacol.* **2014**, *387* (6), 505–521.
(36) Liu, S.; Misquitta, Y. R.; Olland, A.; Johnson, M. A.; Kelleher, K. S.; Kriz, R.; Lin, L. L.; Stahl, M.; Mosyak, L. Crystal Structure of a Human IκB Kinase β Asymmetric Dimer. *J. Biol. Chem.* **2013**, *288* (31), 22758–22767.
(37) Dong, T.; Li, C.; Wang, X.; Dian, L.; Zhang, X.; Li, L.; Chen, S.; Cao, R.; Li, L.; Huang, N.; et al. Ainsliadimer A Selectively Inhibits IKKα/β by Covalently Binding a Conserved Cysteine. *Nat. Commun.* **2015**, *6* (1), 6522.
(38) Kwok, B. H. B.; Koh, B.; Ndubuisi, M. I.; Elofsson, M.; Crews, C. M. The Anti-Inflammatory Natural Product Parthenolide from the Medicinal Herb Feverfew Directly Binds to and Inhibits IκB Kinase. *Chem. Biol.* **2001**, *8* (8), 759–766.
(39) Burch, J. D.; Lau, K.; Barker, J. J.; Brookfield, F.; Chen, Y.; Chen, Y.; Eigenbrot, C.; Ellebrandt, C.; Ismaili, M. H. A.; Johnson, A.; et al. Property- and Structure-Guided Discovery of a Tetrahydroindazole Series of Interleukin-2 Inducible T-Cell Kinase Inhibitors. *J. Med. Chem.* **2014**, *57* (13), 5714–5727.
(40) Zapf, C. W.; Gerstenberger, B. S.; Xing, L.; Limburg, D. C.; Anderson, D. R.; Caspers, N.; Han, S.; Aulabaugh, A.; Kurumbail, R.; Shakya, S.; et al. Covalent Inhibitors of Interleukin-2 Inducible T Cell Kinase (Itk) with Nanomolar Potency in a Whole-Blood Assay. *J. Med. Chem.* **2012**, *55* (22), 10047–10063.
(41) Goedken, E. R.; Argiriadi, M. A.; Banach, D. L.; Fiamengo, B. A.; Foley, S. E.; Frank, K. E.; George, J. S.; Harris, C. M.; Hobson, A. D.; Ihle, D. C.; et al. Tricyclic Covalent Inhibitors Selectively Target Jak3 through an Active Site Thiol. *J. Biol. Chem.* **2015**, *290* (8), 4573–4589.
(42) Tan, L.; Akahane, K.; McNally, R.; Reyskens, K. M. S. E.; Ficarro, S. B.; Liu, S.; Herter-Sprie, G. S.; Koyama, S.; Pattison, M. J.; Labella, K.; et al. Development of Selective Covalent Janus Kinase 3 Inhibitors. *J. Med. Chem.* **2015**, *58* (16), 6589–6606.
(43) Shaw, D.; Wang, S. M.; Villaseñor, A. G.; Tsing, S.; Walter, D.; Browner, M. F.; Barnett, J.; Kuglstatter, A. The Crystal Structure of JNK2 Reveals Conformational Flexibility in the MAP Kinase Insert and Indicates Its Involvement in the Regulation of Catalytic Activity. *J. Mol. Biol.* **2008**, *383* (4), 885–893.
(44) Zhang, T.; Inesta-Vaquera, F.; Niepel, M.; Zhang, J.; Ficarro, S. B.; Machleidt, T.; Xie, T.; Marto, J. A.; Kim, N.; Sim, T.; et al. Discovery of Potent and Selective Covalent Inhibitors of JNK. *Chem. Biol.* **2012**, *19* (1), 140–154.
(45) Zheng, K.; Iqbal, S.; Hernandez, P.; Park, H.; LoGrasso, P. V.; Feng, Y. Design and Synthesis of Highly Potent and Isoform Selective JNK3 Inhibitors: SAR Studies on Aminopyrazole Derivatives. *J. Med. Chem.* **2014**, *57* (23), 10013–10030.
(46) Ohren, J. F.; Chen, H.; Pavlovsky, A.; Whitehead, C.; Zhang, E.; Kuffa, P.; Yan, C.; McConnell, P.; Spessard, C.; Banotai, C.; et al. Structures of Human MAP Kinase Kinase 1 (MEK1) and MEK2 Describe Novel Noncompetitive Kinase Inhibition. *Nat. Struct. Mol. Biol.* **2004**, *11* (12), 1192–1197.
(47) Malakhova, M.; D'Angelo, I.; Kim, H.-G.; Kurinov, I.; Bode, A. M.; Dong, Z. The Crystal Structure of the Active Form of the C-Terminal Kinase Domain of Mitogen- and Stress-Activated Protein Kinase 1. *J. Mol. Biol.* **2010**, *399* (1), 41–52.
(48) Westwood, I.; Cheary, D.-M.; Baxter, J. E.; Richards, M. W.; van Montfort, R. L. M.; Fry, A. M.; Bayliss, R. Insights into the Conformational Variability and Regulation of Human Nek2 Kinase. *J. Mol. Biol.* **2009**, *386* (2), 476–485.
(49) Henise, J. C.; Taunton, J. Irreversible Nek2 Kinase Inhibitors with Cellular Activity. *J. Med. Chem.* **2011**, *54* (12), 4133–4146.
(50) Liang, L.; Yan, X.-E.; Yin, Y.; Yun, C.-H. Structural and Biochemical Studies of the PDGFRA Kinase Domain. *Biochem. Biophys. Res. Commun.* **2016**, *477* (4), 667–672.
(51) Li, D.; Fu, T.-M.; Nan, J.; Liu, C.; Li, L.-F.; Su, X.-D. Structural Basis for the Autoinhibition of the C-Terminal Kinase Domain of Human RSK1. *Acta Crystallogr. Sect. D Biol. Crystallogr.* **2012**, *68* (6), 680–685.
(52) Cohen, M. S.; Zhang, C.; Shokat, K. M.; J., T. Structural Bioinformatics-Based Design of Selective, Irreversible Kinase Inhibitors. *Science (80-.).* **2005**, *308* (5726), 1318–1321.
(53) Malakhova, M.; Tereshko, V.; Lee, S.-Y.; Yao, K.; Cho, Y.-Y.; Bode, A.; Dong, Z. Structural Basis for Activation of the Autoinhibitory C-Terminal Kinase Domain of P90 RSK2. *Nat. Struct. Mol. Biol.* **2008**, *15* (1), 112–113.
(54) Wu, J.; Powell, F.; Larsen, N. A.; Lai, Z.; Byth, K. F.; Read, J.; Gu, R.-F.; Roth, M.; Toader, D.; Saeh, J. C.; et al. Mechanism and In Vitro Pharmacology of TAK1 Inhibition by (5 Z)-7-Oxozeaenol. *ACS Chem. Biol.* **2013**, *8* (3), 643–650.
(55) Tan, L.; Gurbani, D.; Weisberg, E. L.; Hunter, J. C.; Li, L.; Jones, D. S.; Ficarro, S. B.; Mowafy, S.; Tam, C.-P.; Rao, S.; et al. Structure-Guided Development of Covalent TAK1 Inhibitors. *Bioorg. Med. Chem.* **2016**, *25* (3), 838–846.
(56) McTigue, M.; Murray, B. W.; Chen, J. H.; Deng, Y.-L.; Solowiej, J.; Kania, R. S. Molecular Conformations, Interactions, and Properties Associated with Drug Efficiency and Clinical Performance among VEGFR TK Inhibitors. *Proc. Natl. Acad. Sci.* **2012**, *109* (45), 18281–18289.
(57) Wissner, A.; Fraser, H. L.; Ingalls, C. L.; Dushin, R. G.; Floyd, M. B.; Cheung, K.; Nittoli, T.; Ravi, M. R.; Tan, X.; Loganzo, F. Dual Irreversible Kinase Inhibitors: Quinazoline-Based Inhibitors Incorporating Two Independent Reactive Centers with Each Targeting Different Cysteine Residues in the Kinase Domains of EGFR and VEGFR-2. *Bioorg. Med. Chem.* **2007**, *15* (11), 3635–3648.
(58) Thurlkill, R. L.; Grimsley, G. R.; Scholtz, J. M.; Pace, C. N. PK Values of the Ionizable Groups of Proteins. *Protein Sci.* **2006**, *15* (5), 1214–1218.